# Supplementary Materials for

**Speed-up, slowdown, and redirection of ice flow on neighbouring ice streams in the Pope, Smith and Kohler region of West Antarctica.**

Selley *et al.*

*Corresponding author. Email: H.L.Selley@leeds.ac.uk

**This file includes:**

Figs. S1 to S4
Tables S1 to S2
Equation S1

**Fig. S1.**

**Changes in flow direction and ice flux on Dotson and Crosson ice shelves.** Panels **A-C** show **(A)** flow direction, **(B)** cumulative upstream ice flux and **(C)** flowlines in 2005. Panels **D-F** are the same for 2019. **(G)** Change in flow direction in 2019 compared to 2005. **(H)** Change in cumulative upstream ice flux in 2019 compared to 2005. Panels **(I)** and **(J)** show flow direction change and flow vectors in sub-regions near **(I)** the grounding line of Kohler East Glacier and **(J)** the division between Kohler West and Kohler East. The upstream ice flux in panels **(B)** and **(E)** are calculated along the flow lines shown in panels **(C)** and **(D),** respectively.

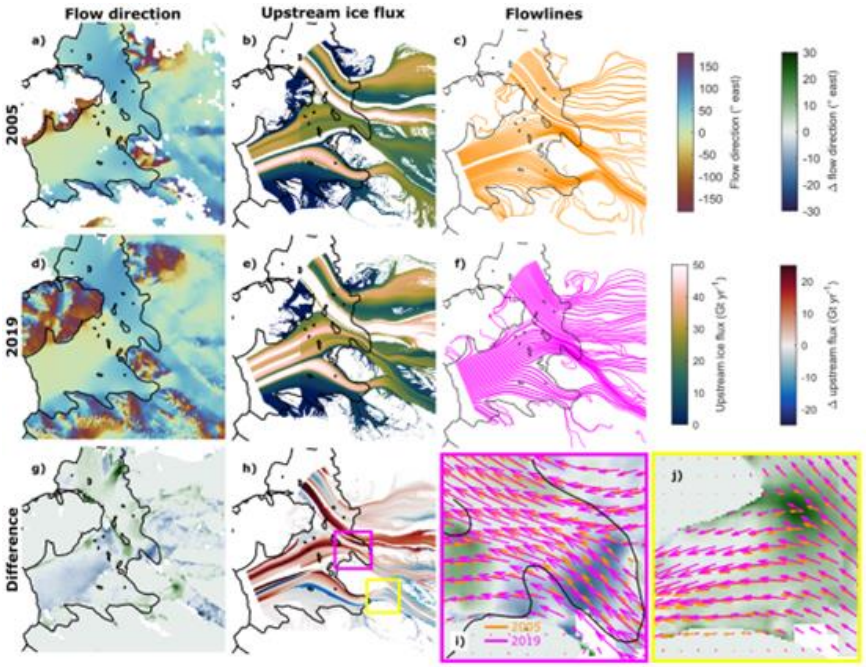

**Fig. S2.**
**Observed area of damage behind the compressive arch on the Crosson Ice Shelf from MODIS imagery (black) and the distance to Bear Peninsula from the crack on the Crosson Ice Shelf (blue).**

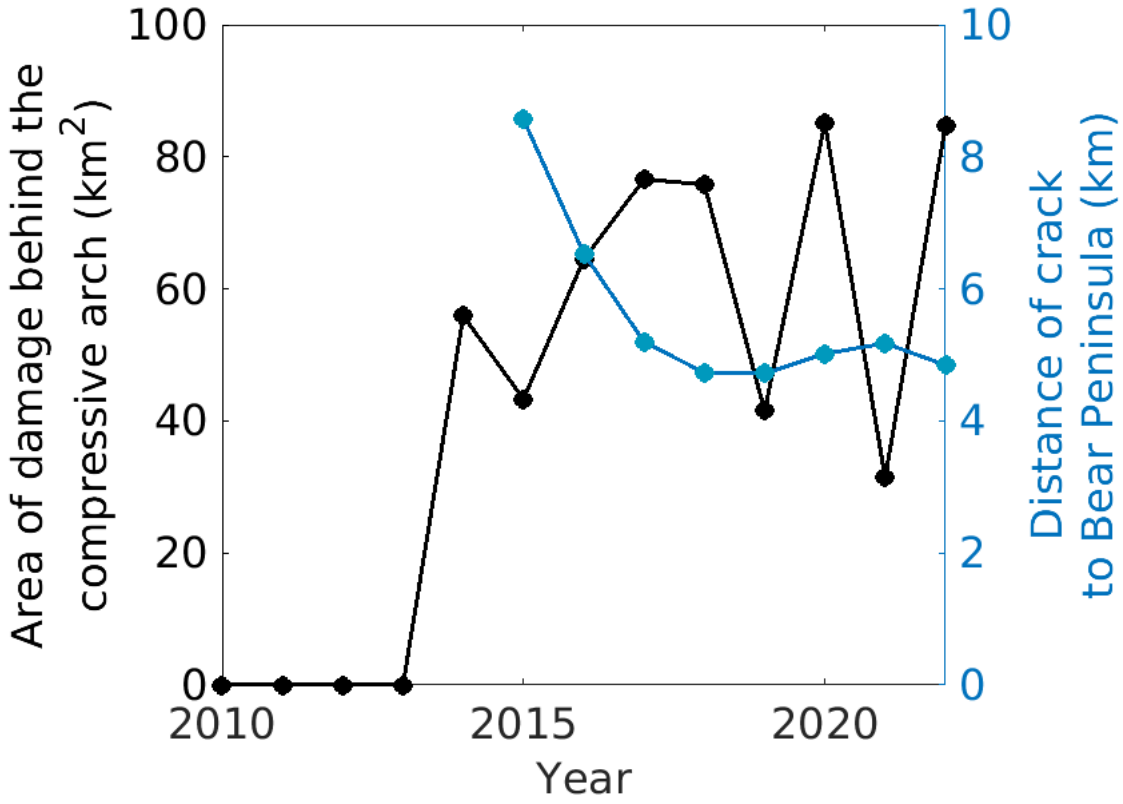


**Fig. S3.**

**Observed ice speed of the Pope, Smith East, Smith West, Kohler glaciers (PSK) and Crosson Ice Shelf and the associated error estimate (right).** Satellite observations included in each annual velocity map are outlined in Table S1. The grounding line location (solid black line), the inland limit of the drainage basin (solid grey line) and the location of the 4 flow lines (dashed black lines) are also shown. The measurements are superimposed over Bedmachine bedrock topography (Morlighem et al., 2011).

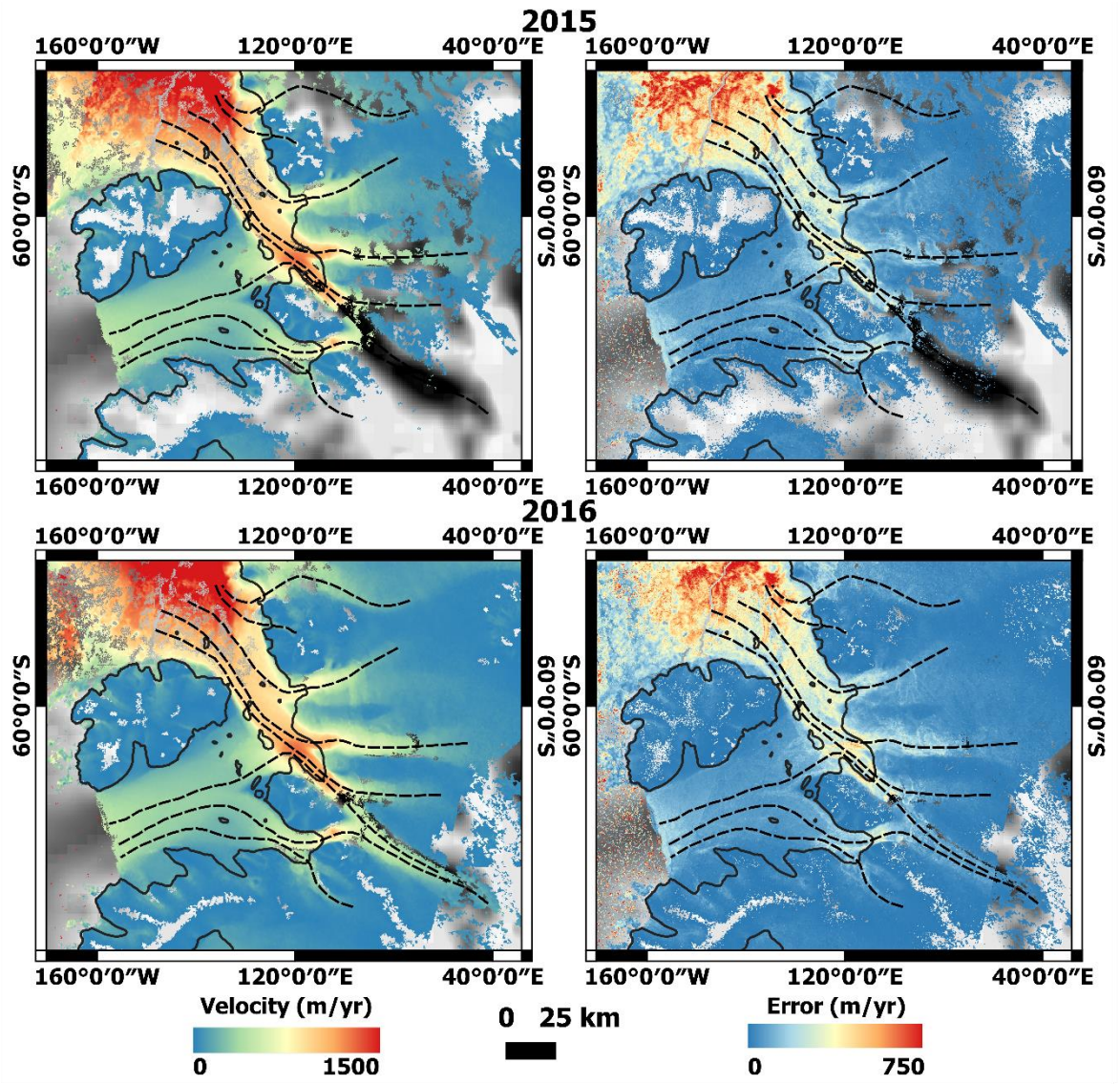
2015
2016
160°0′0″W
120°0′0″E
40°0′0″E
60°0′0″S
Velocity (m/yr)
0
1500
0 25 km
Error (m/yr)
0
750

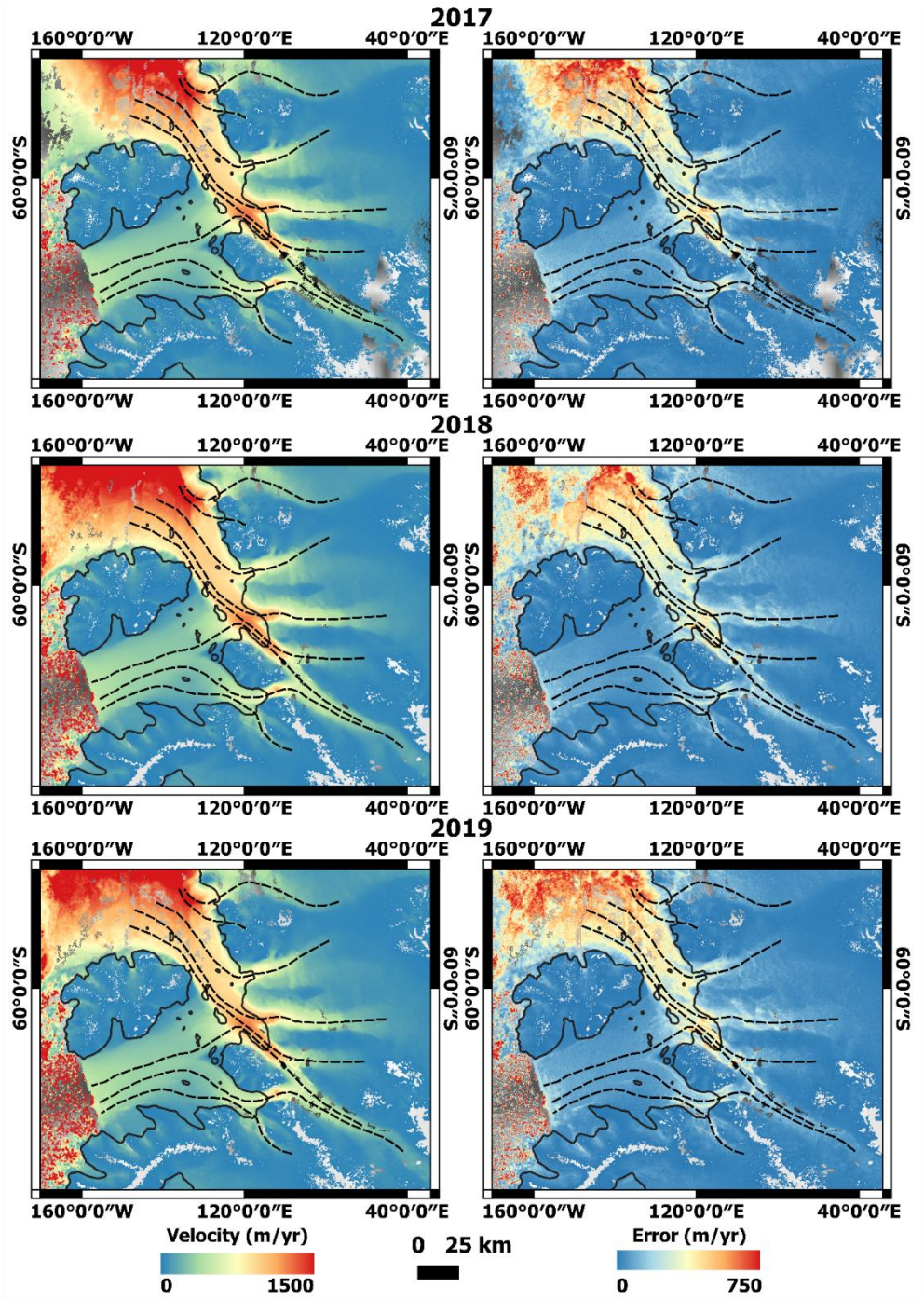
2017
2018
2019
160°0′0″W
120°0′0″E
40°0′0″E
60°0′0″S
Velocity (m/yr)
0
1500
0 25 km
Error (m/yr)
0
750

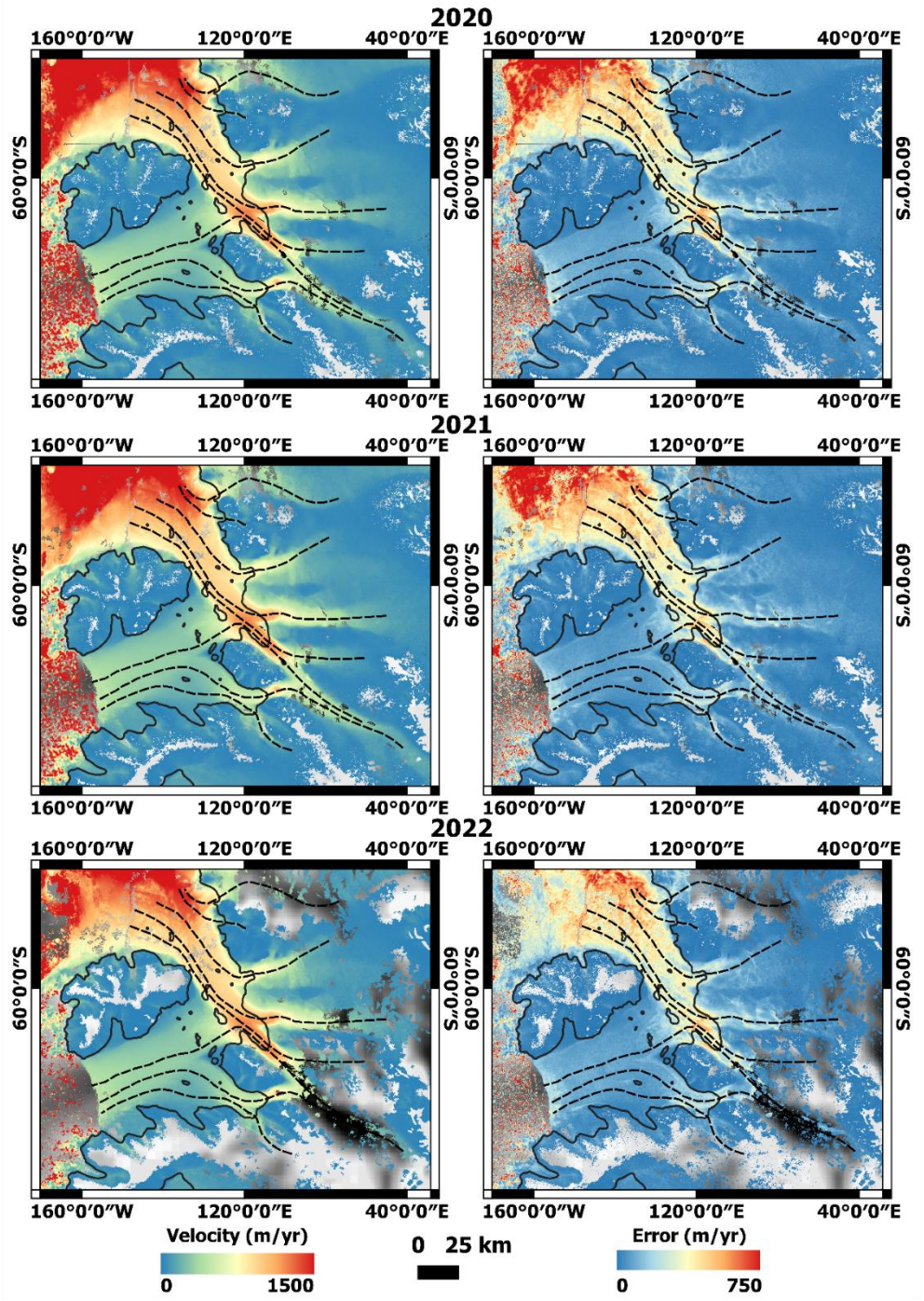
2020
2021
2022
160°0′0″W
120°0′0″E
40°0′0″E
60°0′0″S
Velocity (m/yr)
0
1500
0 25 km
Error (m/yr)
0
750

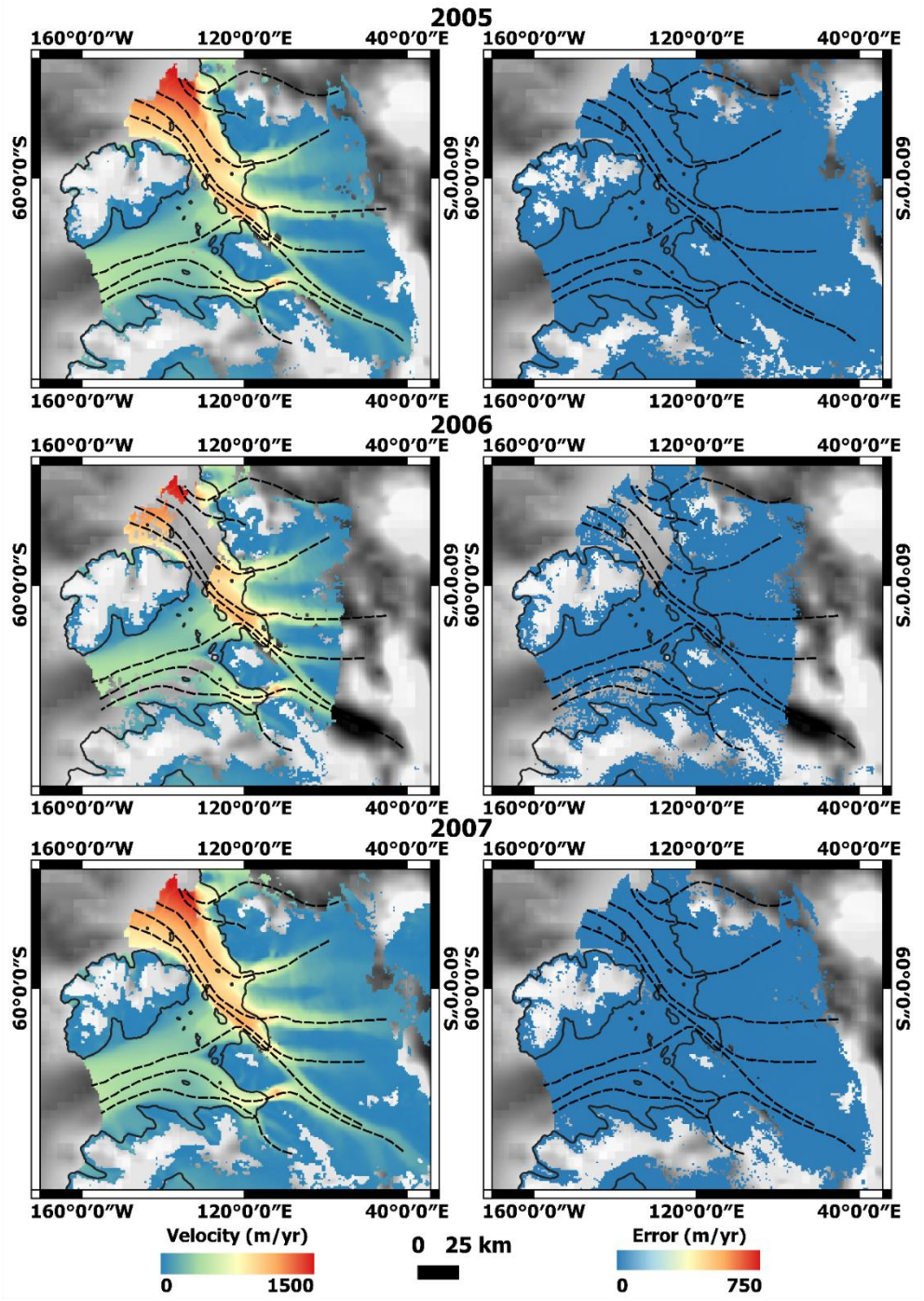
2005
2006
2007
160°0′0″W
120°0′0″E
40°0′0″E
60°0′0″S
Velocity (m/yr)
0
1500
0 25 km
Error (m/yr)
0
750

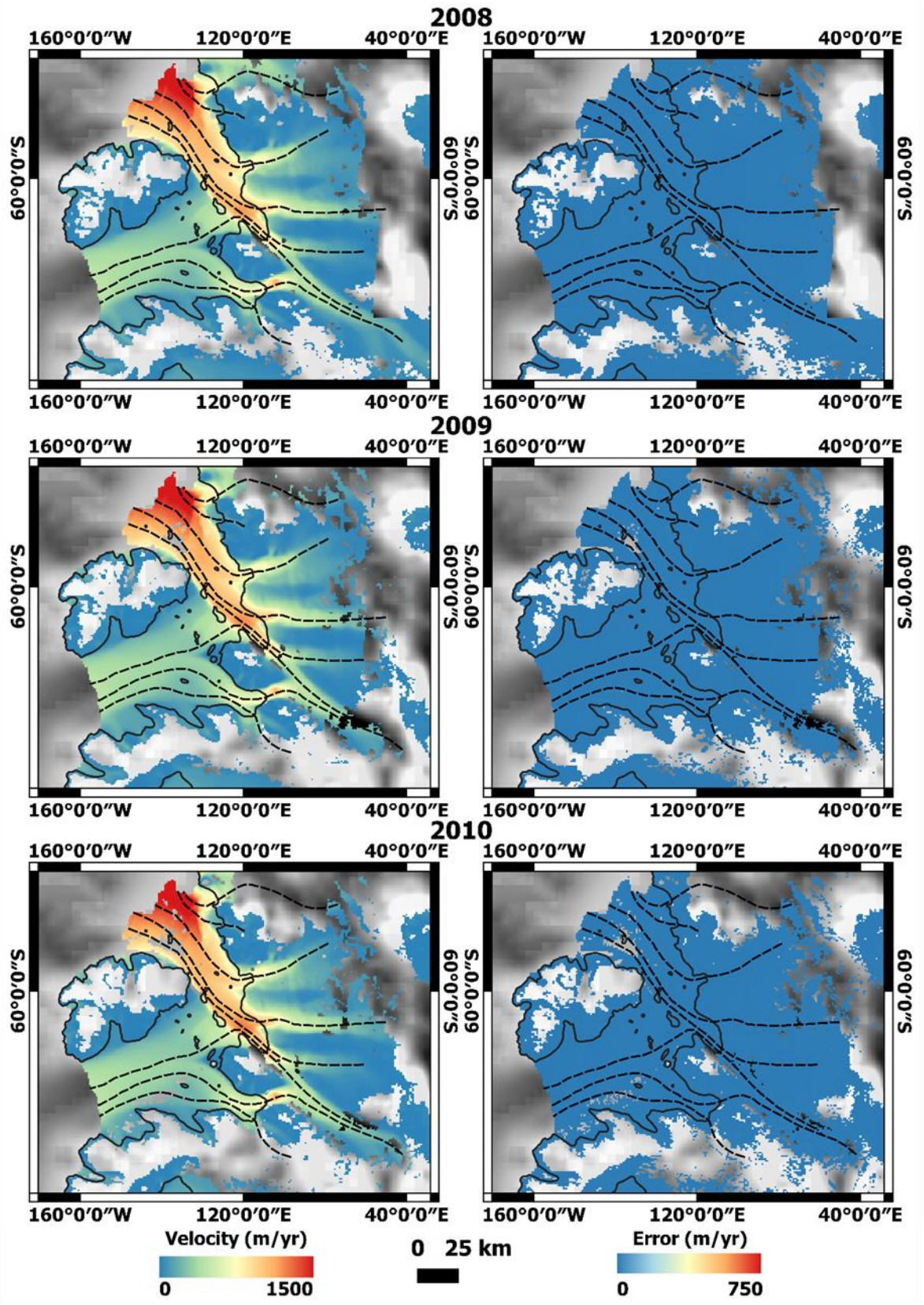
2008
2009
2010
160°0′0″W
120°0′0″E
40°0′0″E
60°0′0″S
Velocity (m/yr)
0
1500
0 25 km
Error (m/yr)
0
750

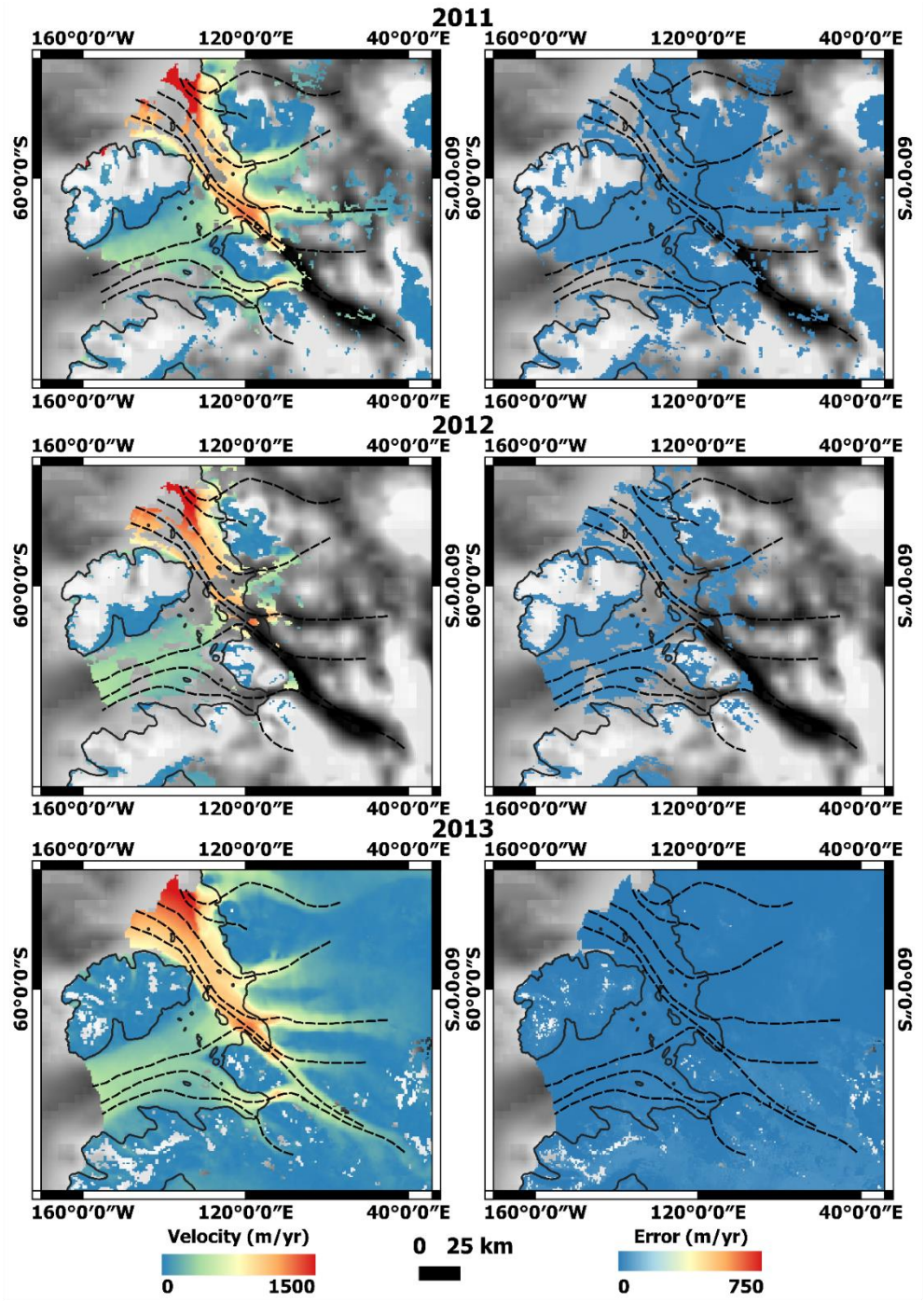
2011
2012
2013
160°0′0″W
120°0′0″E
40°0′0″E
60°0′0″S
Velocity (m/yr)
0
1500
0 25 km
Error (m/yr)
0
750

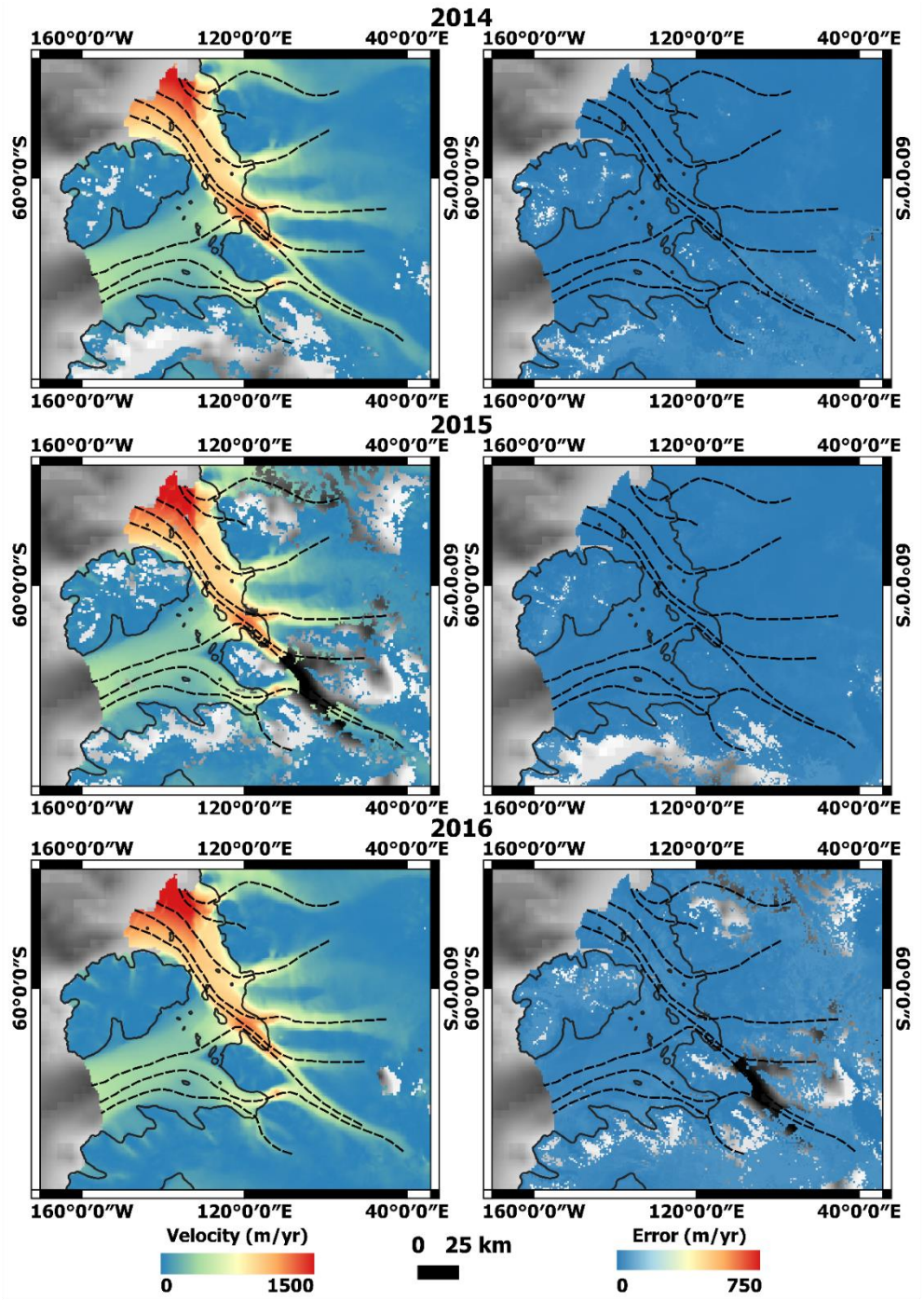
2014
2015
2016
160°0′0″W
120°0′0″E
40°0′0″E
60°0′0″S
Velocity (m/yr)
0
1500
0 25 km
Error (m/yr)
0
750

**Table S1.**

Summary of flow direction changes in the regions of interest identified in Figure 4 based on ice speed and flow direction data, which clearly has been a progressive change in flow direction over time, particularly since 2009 at ROI2.

| Time | ROI 1 | | ROI 2 | |
|---|---|---|---|---|
| | Flow Direction (degrees east of north) | Error (degrees) | Flow Direction (degrees east of north) | Error (degrees) |
| '30-Dec-1996' | 25.06 | 0.09 | 30.19 | 0.18 |
| '30-Dec-2000' | 26.45 | 0.26 | 23.90 | 0.69 |
| '30-Dec-2005' | 26.33 | 0.11 | 25.94 | 0.21 |
| '30-Dec-2006' | 26.42 | 0.21 | 25.54 | 0.45 |
| '30-Dec-2007' | 25.30 | 0.12 | 26.74 | 0.21 |
| '30-Dec-2008' | 25.39 | 0.16 | 25.51 | 0.32 |
| '30-Dec-2009' | 25.89 | 0.13 | 28.31 | 0.20 |
| '30-Dec-2010' | 25.70 | 0.11 | 30.73 | 0.19 |
| '30-Dec-2011' | 25.72 | 0.61 | 31.85 | 1.35 |
| '30-Dec-2012' | 23.39 | 0.83 | 32.47 | 1.78 |
| '30-Dec-2013' | 25.33 | 0.13 | 34.64 | 0.62 |
| '30-Dec-2014' | 24.80 | 0.23 | 34.60 | 0.67 |
| '30-Dec-2015' | 24.54 | 0.44 | 34.50 | 0.86 |
| '30-Dec-2016' | 24.04 | 0.16 | 35.01 | 0.36 |
| '30-Dec-2017' | 23.34 | 0.07 | 37.00 | 0.13 |
| '30-Dec-2018' | 23.10 | 0.07 | 37.82 | 0.13 |
| '30-Dec-2019' | 22.79 | 0.06 | 38.41 | 0.12 |

**Table S2.** Input satellite data used to measure ice speed from 2005.06.01 to 2022.12.31, for all 16 annual velocity maps.

| Annual Velocity Map Name | Satellite | Data Type | Time Period Covered (YYYY.MM.DD) | |
|---|---|---|---|---|
| 2005-2006 | MEaSUREs data represent an average of the following satellite imagery: ALOS, ENVISAT, LANDSAT-8, RADARSAT-1, RADARSAT-2, Sentinel-1A, Sentinel-1B, TDX and TSX | SAR and Optical | 2005.06.01 | 2006.05.30 |
| 2006-2007 | | | 2006.06.01 | 2007.05.30 |
| 2007-2008 | | | 2007.06.01 | 2008.05.30 |
| 2008-2009 | | | 2008.06.01 | 2009.05.30 |
| 2009-2010 | | | 2009.06.01 | 2010.05.30 |
| 2010-2011 | | | 2010.06.01 | 2011.05.30 |
| 2011-2012 | | | 2011.06.01 | 2012.05.30 |
| 2012-2013 | | | 2012.06.01 | 2013.05.30 |
| 2013-2014 | | | 2013.06.01 | 2014.05.30 |
| 2014-2015 | | | 2014.06.01 | 2015.05.30 |
| 2015-2016 | | | 2015.06.01 | 2016.05.30 |
| 2016-2017 | | | 2016.06.01 | 2017.05.30 |
| S1–2015 | Sentinel-1A and Sentinel-1B | SAR | 2015.01.01 | 2015.12.31 |
| S1-2016 | | | 2016.01.01 | 2016.12.31 |
| S1-2017 | | | 2017.01.01 | 2017.12.31 |
| S1-2018 | | | 2018.01.01 | 2018.12.31 |
| S1 -2019 | | | 2019.01.01 | 2019.12.31 |
| S1-2020 | | | 2020.01.01 | 2020.12.31 |
| S1-2021 | | | 2021.01.01 | 2021.12.31 |
| S1-2022 | | | 2022.01.01 | 2022.12.31 |

**Equation S1:** Equation used to calculate deformation with the initial ice thickness and surface slope, then calculated it again with the new thickness and surface slope.

$$U = \left(2 * A/(n+1)\right) * (\rho_i * g * \ \alpha * H)^n * H$$

H = ice thickness

A = rate factor for ice (9.3e-25; s^-1 Pa^-3)

n = flow law exponent (3)

$\rho_i$ = ice density (917 kg/$m^3$)

g = acceleration due to gravity (9.81 m/s/s)

$\alpha$ = sin of the surface slope